https://doi.org/10.48048/tis.2022.5770

Effects of Angle and Rate of Twist via Pre-Torsional Deformation on Tensile Properties and Hardness of Hot-Rolled, Low-Alloy Steel Rods

Pawat Jantasorn and Ukrit Thamma*

Department of Mechanical Engineering Technology, College of Industrial Technology, King Mongkut's University of Technology North Bangkok, Bangkok 10800, Thailand

(*Corresponding author's e-mail: ukrit.t@cit.kmutnb.ac.th)

Received: 8 July 2021, Revised: 4 August 2021, Accepted: 8 August 2021

Abstract

The effects of twist angle and twist rate during the pre-torsional deformation on tensile and hardness properties of hot-rolled SCM415 low-alloy steel were investigated. Hot-rolled SCM415 round tensile specimens were pre-torsioned using a free-end torsion machine to 36, 72, 144 and 288 degrees at 2 different twist rates of 0.1 and 30 rpm. As the angle and the rate of twist increased, yield strength and ultimate tensile strength increased with a tradeoff in a reduction in ductility. The relationship of true stress and true strain within the uniform plastic deformation were well described by a power law. The strength coefficient and strain hardening exponent obtained from the power-law curve fitting decreased with increasing twist angle and higher twist rate, suggesting that higher shear strain and shear strain rate led to a decrease in work hardening capacity. The local hardness after pre-torsional deformation showed a positive gradient from specimens' centers to their surfaces along the radial direction. Also, the local hardness at the same radial position increased with the increasing angle and rate of twist. The average grain sizes were uniform along the radial direction and were comparable for all pre-torsional conditions. The strengthening mechanism via pre-torsional deformation of hot-rolled SCM415 was shown to be dominated by the strain hardening effect.

Keywords: Pre-torsional deformation, Cold forming, Tensile properties, Hardness, Low-alloy steel

Introduction

Cold forming processes such as cold rolling [1,2,3], cold drawing [4,5], cold extrusion [6,7] are metal fabrication techniques in which metals are shaped below their recrystallization temperature. As the amount of plastic deformation increases during cold forming, the strength and hardness of the formed metal parts increases while its ductility and toughness decrease. The changes in mechanical properties after the cold forming process are caused by strain hardening where an increase in dislocation density and a higher degree of dislocation entanglement within grains' interior result in the hindrance of dislocation motions [8,9]. Since slip within the crystallographic structure of metals directly involves dislocation motions, by obstructing dislocation motions, higher stress is required to induce plastic deformation, enhancing strength and hardness in metals [10].

Strain hardening is not the only mechanism that leads to strengthening after cold forming in metals. Another strengthening mechanism called grain-size strengthening applies an increase in grain boundaries via grain-size reduction through grain refinement to further impede dislocation motions [10,11]. Recently, severe plastic deformation (SPD), a category of cold forming involving the exertion of high strains into bulk metal parts, has shown promising results in creating ultra-high strength parts by inducing bulk ultrafine grains (UFG) with less than 1 μm in grain size [12]. Common SPD processes are accumulative roll bonding (ARB), multi-directional forging (MDF), equal-channel angular pressing (ECAP), twist extrusion (TE), and high-pressure torsion (HPT) [13]. Especially, torsional SPD processes, such as TE and HPT, have been gaining traction in research studies since they can generate a relatively higher plastic deformation with minimum risk of rupture or strain localization in comparison to compression or tension [11,14]. Wang *et al*. showed a gradient in microstructural evolution and hardening as a function of the plastic shear strain of pure copper after torsion deformation [11]. In austenitic stainless steel, torsional deformation of coarse grain 304 stainless steel was able to promote higher martensite transformation compared to ultrafine grain specimens, leading to improved overall mechanical properties [15]. Chen *et al.* found that the number of torsional deformation directions (i.e., unidirectional or bidirectional) can lead

to different failure behaviors, microstructural gradients, and tensile/hardness properties of pure titanium rods [16].

SCM415 steel is one of the most versatile low-alloy structural steel in the automotive industry. The raw starting materials of SCM415 steel are commonly in the hot-rolled state before going into various secondary manufacturing processes to make automotive parts such as transmission, camshaft, mechanical joints, and gear wheel, etc. These secondary processes heavily involve cold forming to create desired shape and dimensions out of hot-rolled SCM415 steel. This present study aims to provide a deeper understanding of the effects of pre-torsional deformation on tensile and hardness properties of hot-rolled SCM415 steel, which can be used as a foundation of SPD applications for low-alloy steels in the future.

Materials and methods

Materials and fabrication of test specimens

Commercial hot-rolled SCM415 steel rods were acquired as raw materials in this study. SCM415 steel is based on the Japanese Industrial Standard (JIS) with the chemical composition described in **Table 1**. The chemical composition of the acquired materials was confirmed using optical emission spectroscopy (OES).

Table 1 Chemical composition of SCM415 low-alloy steel based on Japanese Industrial Standard (JIS).

Element	Chemical composition (wt%)
Carbon (C)	0.13 - 0.18
Silicon (Si)	0.15 - 0.35
Manganese (Mn)	0.60 - 0.85
Phosphorous (P)	<0.03
Sulfur (S)	<0.03
Nickel (Ni)	<0.25
Chromium (Cr)	0.90 - 1.20
Molybdenum (Mo)	0.15 - 0.30
Copper (Cu)	<0.30
Iron (Fe)	Balanced

Acquired hot-rolled SCM415 rods were machined using computerized numerical control (CNC) lathe into round tensile specimens based on ASTM E8/E8M (Standard Test Methods for Tension Testing of Metallic Materials) with the diameter of 6.0 ± 0.1 mm and the gauge length of 30.0 ± 0.1 mm, as illustrated in **Figure 1**.

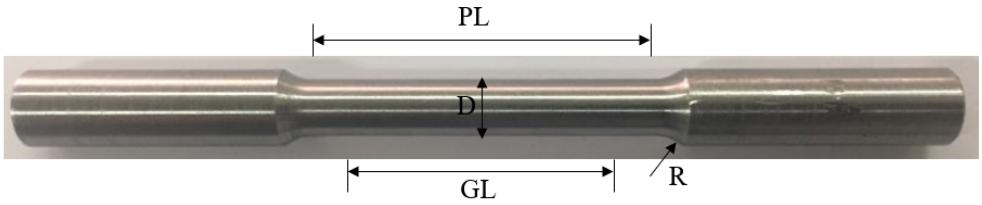

GL (gauge length) = 30.0 ± 0.1 mm
D (diameter) = 6.0 ± 0.1 mm
PL (length of reduced parallel section) = 36 mm
R (radius of fillet) = 6 mm

Figure 1 Shape and dimensions of SCM415 round tensile specimens based on ASTM E8/E8M.

Pre-torsional deformation

Prepared SCM415 tensile specimens were subjected to pre-torsional deformation using an Ibertest free-end torsion testing machine, as shown in **Figure 2**, where the specimens' free ends were twisted via torsion relative to their fixed ends. Four different pre-torsional angles used to create various degrees of

shear deformation were 36, 72, 144 and 288 degrees, while 2 different rotational speeds of 0.1 and 30 rpm were applied to yield different shear strain rates.

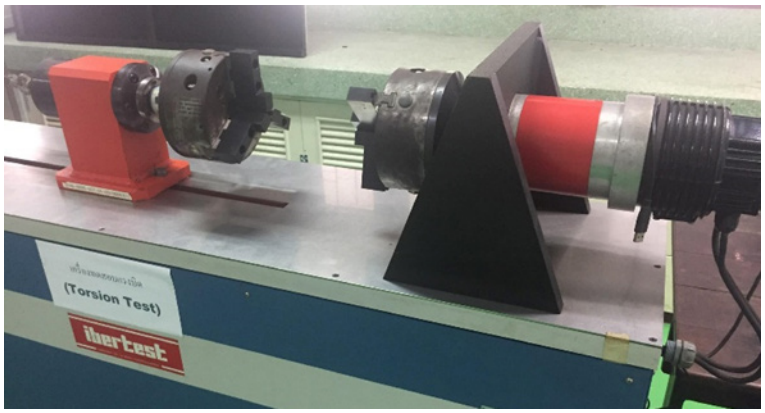

Figure 2 Ibertest free-end torsion machine.

Tensile and hardness tests

SCM415 tensile specimens before and after pre-torsional deformation were subjected to tensile test using an Instron 5569 tensile testing system with a constant crosshead speed of 0.6 mm per min or a constant strain rate of ~2.78×10^{-4} s^{-1}. For precise strain measurement during the tensile tests, a mechanical extensometer was employed and was positioned within the gauge length of all specimens. The tensile tests were repeated on at least 4 different specimens with the same pre-torsional deformation condition to ensure the stringency of the statistical analyses. Both engineering and true stress-strain curves were plotted for all pre-torsional deformation conditions. The local Vicker hardness (HV) along the radial direction of SCM415 tensile specimens before and after pre-torsional deformation was measured using a Future Tech Corp FM-7 Microhardness Tester at a load of 300 g and a loading time of 10 s. The local hardness was measured at various positions away from the specimen's center along its radial direction to its surface. Each measured position was defined as the ratio of the distance (R) from the specimen's axial centerline to its nominal specimen radius (R_0), where $R/R_0 \approx 0.0$ and $R/R_0 \approx 1.0$ represent the positions at the center and the surface of the specimens, respectively. The reported local hardness at each R/R_0 position was an average of ten independent measurements to ensure the stringency of the statistical analyses.

Microstructure observation via light optical microscopy

The microstructures of SCM415 tensile specimens before and after pre-torsional deformation were characterized from the diametrical cross-section using an Olympus GX71 light optical microscope. The specimens were transversely sectioned at the center of the gauge length using a high-speed silicon-carbide (SiC) saw with continuous cooling. Sectioned specimens were mounted in Bakelite, a phenol-formaldehyde resin, at 180 °C and under a pressure of 250 bar. Mounted specimens were ground using SiC abrasive papers up to 1,500 grit number and were polished using 1-µm alumina (Al_2O_3). Polished specimens were then etched using a 2.5 vol% nitric acid (HNO_3) solution. The microstructures of all specimens were observed at 3 different distances away from the specimen's axial centerline along the radial direction in terms of R/R_0 which are approximately 0.0, 0.5 and 1.0. Average grain sizes at different R/R_0 positions of all pre-torsional conditions were analyzed and quantified using the linear intercept method via ImageJ software from at least 4 micrographs to ensure the stringency of the statistical analyses.

Results and discussion

After pre-torsional deformation, the round SCM415 tensile specimens were subjected to tensile tests. The engineering stress-strain curves of specimens before pre-torsional deformation and after pre-torsional deformation to 36, 72, 144 and 288 degrees at 2 different twist rates of 0.1 and 30 rpm are plotted as shown in **Figure 3**. Yield strength (YS) at the strain offset of 0.002, ultimate tensile strength

(UTS), and % elongation at failure (%EL_{max}) of all pre-torsional conditions are summarized in **Table 2**. Based on the engineering stress-strain curves, as the pre-torsional angle increases, both yield and tensile strengths increased while the ductility decreased. With the same pre-torsional angle, specimens subjected to 30-rpm twist rate demonstrated higher yield and tensile strengths with lower ductility compared to those subjected to 0.1-rpm twist rate. Moreover, the differences in mechanical properties created by different twist rates were more noticeable in specimens pre-torsioned to a larger angle.

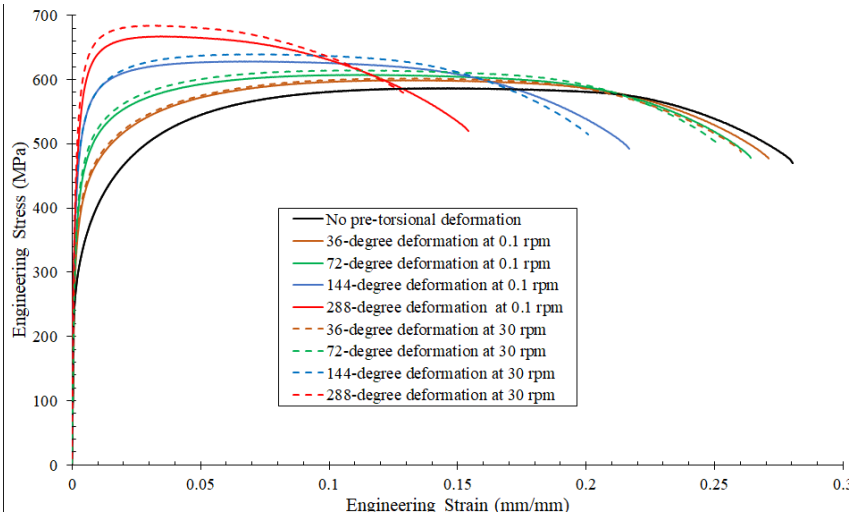

Figure 3 Engineering stress-strain curves of SCM415 specimens for all pre-torsional conditions.

Table 2 Summary of yield strength at 0.002 strain offset, ultimate tensile strength, and % elongation at failure of specimens with different pre-torsional conditions.

Pre-torsional condition	Yield strength (YS) at 0.002 strain offset	Ultimate tensile strength (UTS)	% Elongation at failure (%EL_{max})
No pre-torsional deformation	320.0 ± 5.5 MPa	587.0 ± 2.8 MPa	28.5 ± 0.9 %
36 degrees at 0.1 rpm	387.3 ± 2.5 MPa	598.8 ± 2.0 MPa	27.1 ± 0.5 %
72 degrees at 0.1 rpm	432.7 ± 6.1 MPa	607.4 ± 1.4 MPa	26.4 ± 0.8 %
144 degrees at 0.1 rpm	480.1 ± 14.4 MPa	628.8 ± 2.9 MPa	21.7 ± 0.6 %
288 degrees at 0.1 rpm	547.0 ± 7.9 MPa	667.0 ± 3.1 MPa	15.4 ± 0.4 %
36 degrees at 30 rpm	391.5 ± 5.6 MPa	601.6 ± 5.1 MPa	26.0 ± 0.6 %
72 degrees at 30 rpm	440.8 ± 5.9 MPa	614.1 ± 4.0 MPa	25.1 ± 0.7 %
144 degrees at 30 rpm	492.5 ± 12.9 MPa	640.0 ± 1.9 MPa	20.1 ± 0.5 %
288 degrees at 30 rpm	563.6 ± 11.5 MPa	684.5 ± 3.3 MPa	12.9 ± 0.3 %

The true stress (σ_T) and true strain (ε_T) within the uniform elongation region (before necking, up to UTS) were computed using the engineering stress (σ_E) and engineering strain (ε_E) using the Eqs. (1) and (2) as follows:

$$\sigma_T = \sigma_E(1 + \varepsilon_E) \quad (1)$$

$$\varepsilon_T = ln(1 + \varepsilon_E) \quad (2)$$

True stress-strain curves and the corresponding strain hardening rate curves for all pre-torsional conditions are plotted as shown in **Figures 4(a)** and **4(b)**, respectively. For all pre-torsional conditions, the strain hardening rate was initially high but then rapidly dropped at higher true strain. With increasing shear deformation via pre-torsion to a larger angle, a relatively lower strain hardening rate at the same true strain was observed. Furthermore, a higher twist rate during pre-torsional deformation to the same angle led to a decrease in the strain hardening rate at the same true strain.

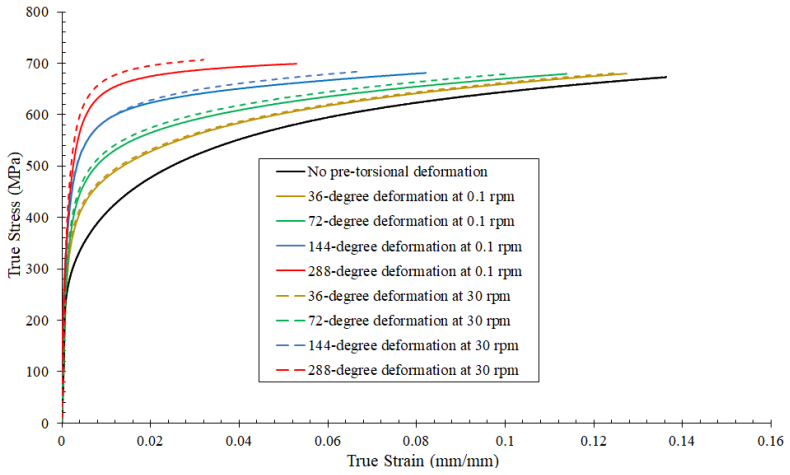

(a)

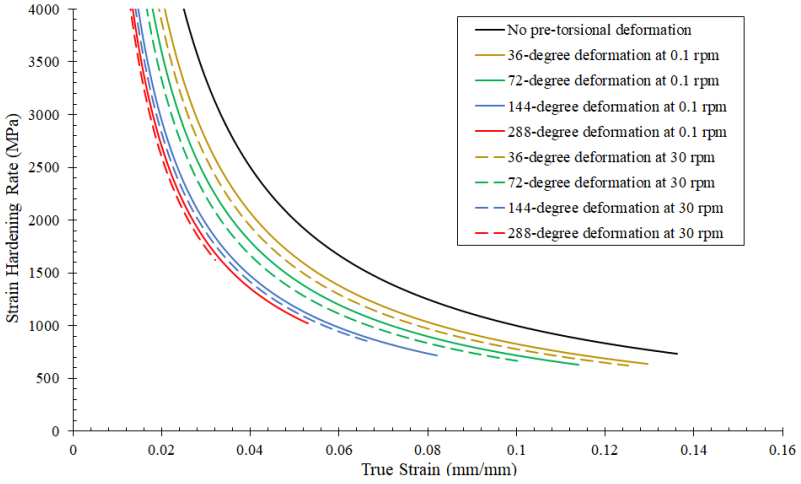

(b)

Figure 4 (a) True stress-strain curves and (b) its corresponding strain hardening rate curves for pre-torsional conditions.

Within the uniform plastic deformation region (from YS to UTS), although the true stress and true strain are in a nonlinear relation, a power law can be applied to represent the true stress-strain relation in the Eq. (3) as follows [17,18]:

$$\sigma_T = K\varepsilon_T^n \tag{3}$$

where K is the strength coefficient, and n is the strain hardening exponent. For all pre-torsional conditions, the experimental tensile results within the uniform plastic deformation were well fitted using the mentioned power-law form with the coefficient of determination (R^2) ranging from 0.9715 to 0.9986, as depicted in **Figure 5**. The power-law parameters, K and n, are summarized in **Table 3**. With increasing

higher degree of shear deformation via larger pre-torsional angle, both K and n values decreased, which implies that pre-torsional deformation reduced work hardening capacity of hot-rolled SCM415 steel. This also correlates with the less rapid strain hardening rate in specimens with a higher degree of shear deformation after pre-torsioned to a relatively larger angle, as illustrated in **Figure 4(b)**.

In addition, UTS determined from the engineer stress-strain curves can be predicted from the strain hardening parameters, K and n. According to Considère, at the maximum load during a tensile test, ε_T is equal to n [19]. Hence, the UTS can be computed using the expression as follows [20]:

$$UTS = K\left(\frac{n}{e}\right)^n$$

The summary of predicted UTS and the corresponding % difference from the experimental UTS for all pre-torsional conditions are presented in **Table 3**. With less than 3 % difference of the predicted UTS from the experimental values, it is confirmed that the power law is an accurate model for representing the relationship of true stress and true strain within the uniform plastic deformation region of hot-rolled SCM415 steel.

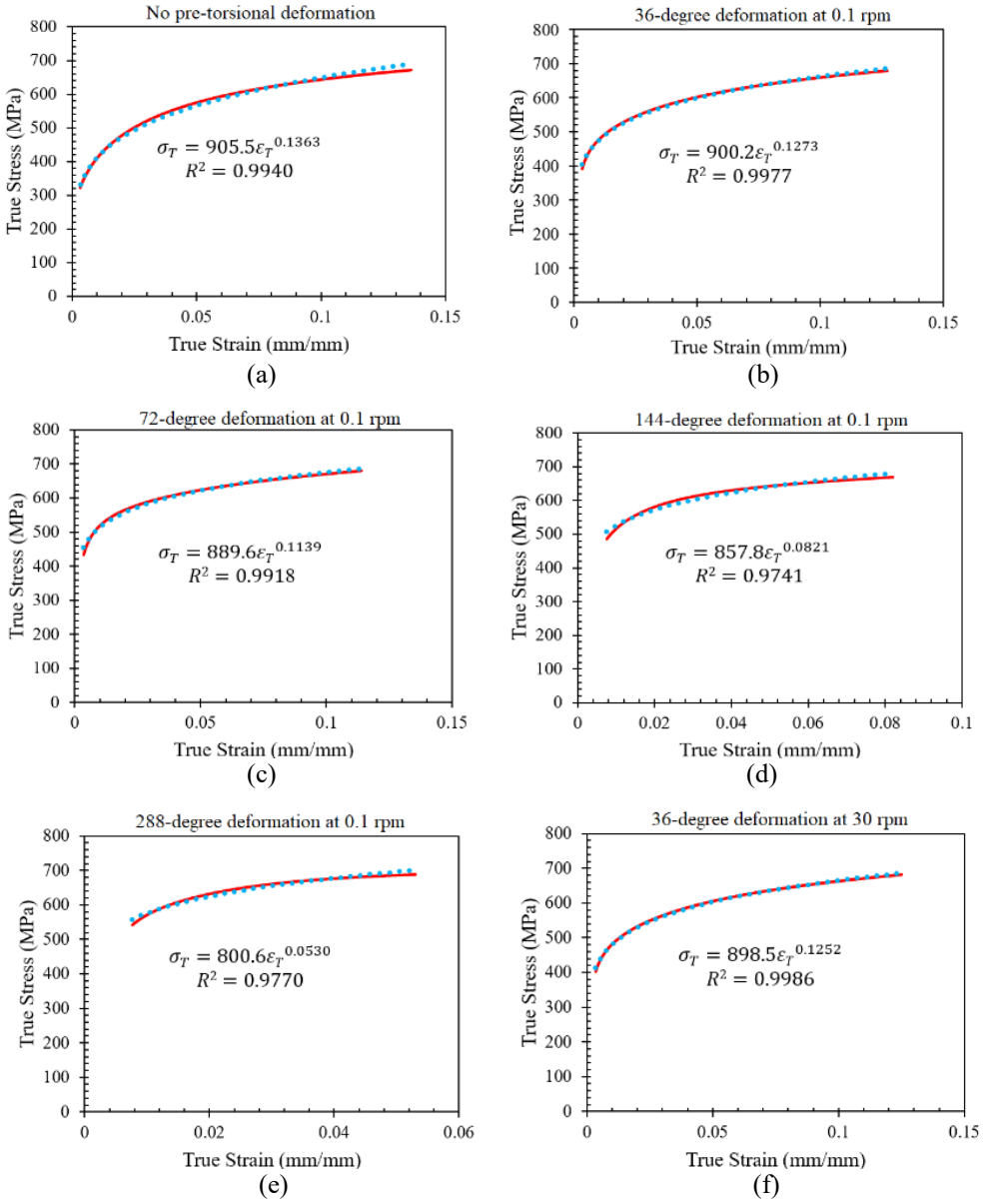

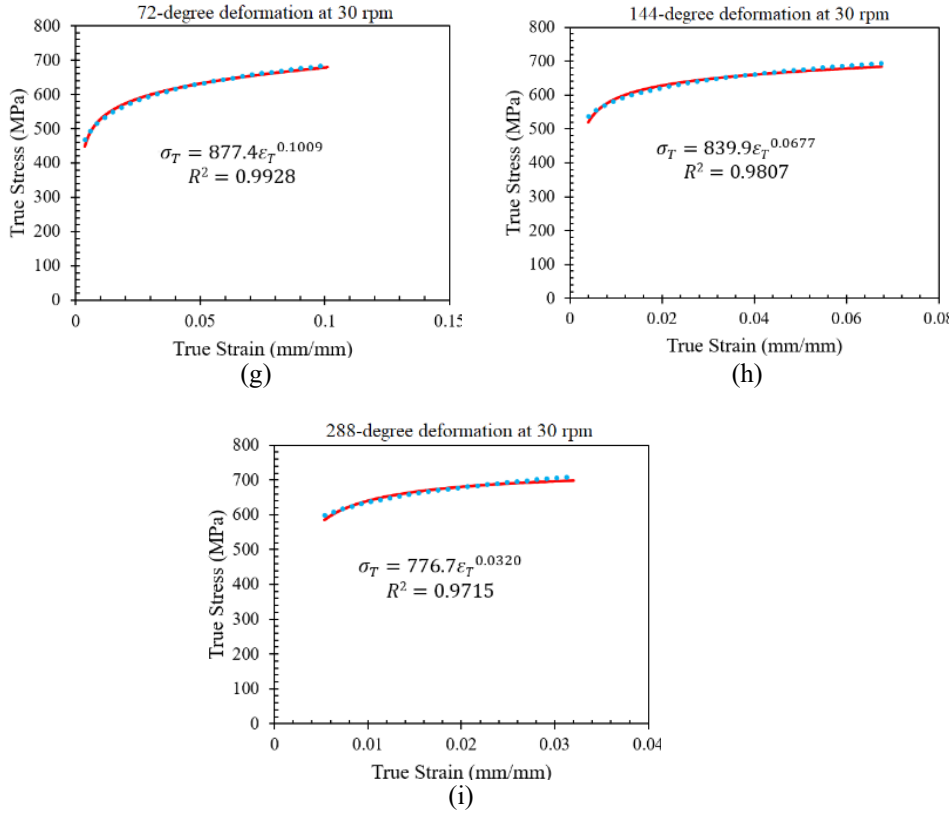

Figure 5 True stress-strain curve within the uniform plastic deformation region (from YS to UTS) curve-fitted using a power law of specimens with pre-torsional deformation of: (a) no pre-torsional deformation (b) 36 degrees at 0.1 rpm (c) 72 degrees at 0.1 rpm (d) 144 degrees at 0.1 rpm (e) 288 degrees at 0.1 rpm (f) 36 degrees at 30 rpm (g) 72 degrees at 30 rpm (h) 144 degrees at 30 rpm (i) 288 degrees at 30 rpm.

Table 3 Summary of power-law curve fitting parameters, strength coefficient (*K*) and strain hardening exponent (*n*), obtained in the uniform plastic deformation region (from YS to UTS) of true stress-strain curves with predicted UTS from *K* and *n* values and % difference from the experimental values.

Pre-torsional condition	Strength coefficient (*K*)	Strain hardening exponent (*n*)	Predicted UTS	% Difference from experimental UTS
No pre-torsional deformation	905.5 MPa	0.1363	602.2 MPa	2.52 %
36 degrees at 0.1 rpm	900.2 MPa	0.1273	609.7 MPa	1.78 %
72 degrees at 0.1 rpm	889.6 MPa	0.1139	619.8 MPa	2.00 %
144 degrees at 0.1 rpm	857.8 MPa	0.0821	643.6 MPa	2.30 %
288 degrees at 0.1 rpm	800.6 MPa	0.0530	649.8 MPa	2.65 %
36 degrees at 30 rpm	898.5 MPa	0.1252	611.2 MPa	1.57 %
72 degrees at 30 rpm	877.4 MPa	0.1009	629.3 MPa	2.42 %
144 degrees at 30 rpm	839.9 MPa	0.0677	654.1 MPa	2.16 %
288 degrees at 30 rpm	776.7 MPa	0.0320	673.8 MPa	1.59 %

Local Vicker hardness (HV) from the center ($R/R_0 \approx 0.0$) to the surface ($R/R_0 \approx 1.0$) along the radial direction of specimens before and after pre-torsional deformation to different angles at the twist rate of 0.1 and 30 rpm are depicted in **Figures 6(a)** and **6(b)**, respectively. The local hardness of the specimens with no pre-torsional deformation was uniform along the radial direction. With pre-torsional deformation,

the local hardness of the specimens increased along the radial direction from their center to their surface. Furthermore, the local hardness at the same R/R_0 position along the radial direction increased as the pre-torsional angle increased. In terms of the twist-rate effect, the local hardness at the same R/R_0 position of specimens pre-torsioned to the same angle increased as the twist rate increased. The difference in the local hardness as a result of different twist rates was found to be more distinct in specimens pre-torsioned to a relatively larger angle.

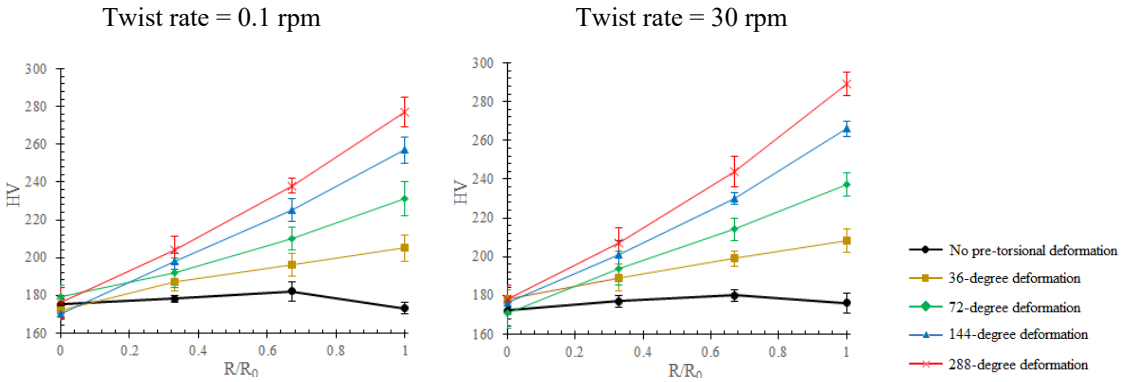

Figure 6 Local Vicker hardness (HV) at different R/R_0 positions along the radial direction of specimens without pre-torsional deformation (black circle) and with pre-torsional deformation to 36 degrees (brown square), 72 degrees (green diamond), 144 degrees (blue triangle), and 288 degrees (red cross) at the twist rate of: (a) 0.1 rpm (b) 30 rpm.

Light optical micrographs of specimens with no pre-torsional deformation, specimens after pre-torsional deformation at 0.1-rpm twist rate, and specimens after pre-torsional deformation at 30-rpm twist rate are shown in **Figures 7 - 9**, respectively. The micrographs were taken at 3 different regions: $R/R_0 \approx$ 0.0, 0.5, and 1.0, where pro-eutectoid α-ferrite (light regions) and pearlite (dark regions) were observed. The average grain sizes of all pre-torsional conditions measured in different R/R_0 regions are summarized in **Table 4**. It was found that the average grain sizes of specimens were uniform along the radial direction and were comparable for all pre-torsional conditions.

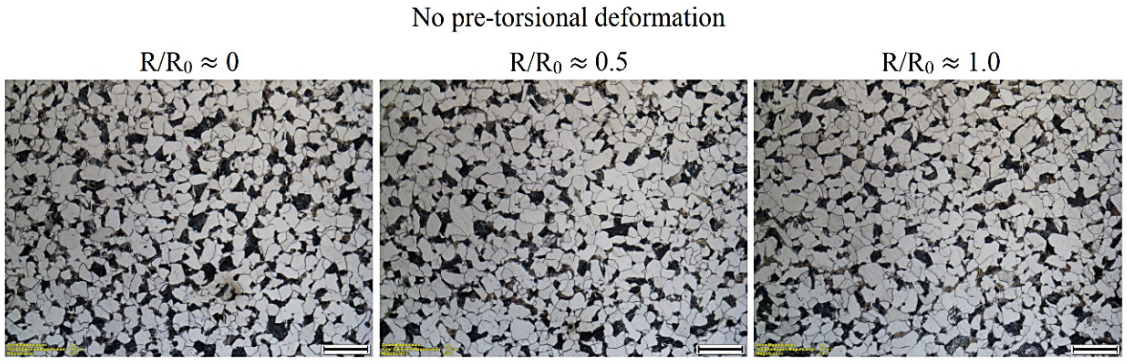

Figure 7 Light optical micrographs at various R/R_0 positions of specimens without pre-torsional deformation (scale bar = 50 μm).

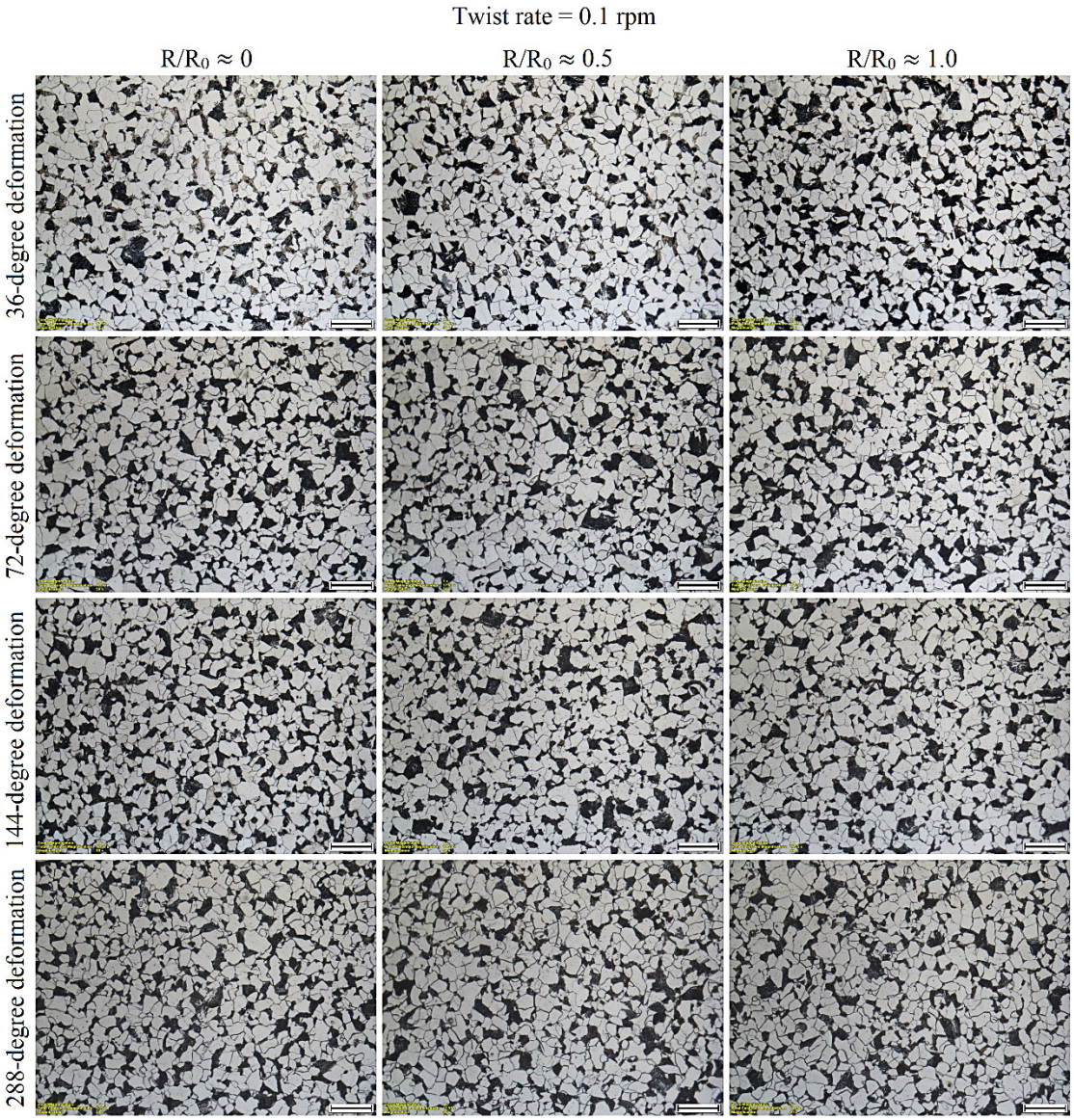

Figure 8 Light optical micrographs at various R/R_0 positions of specimens with pre-torsional deformation to various angles at a twist rate of 0.1 rpm (scale bar = 50 μm).

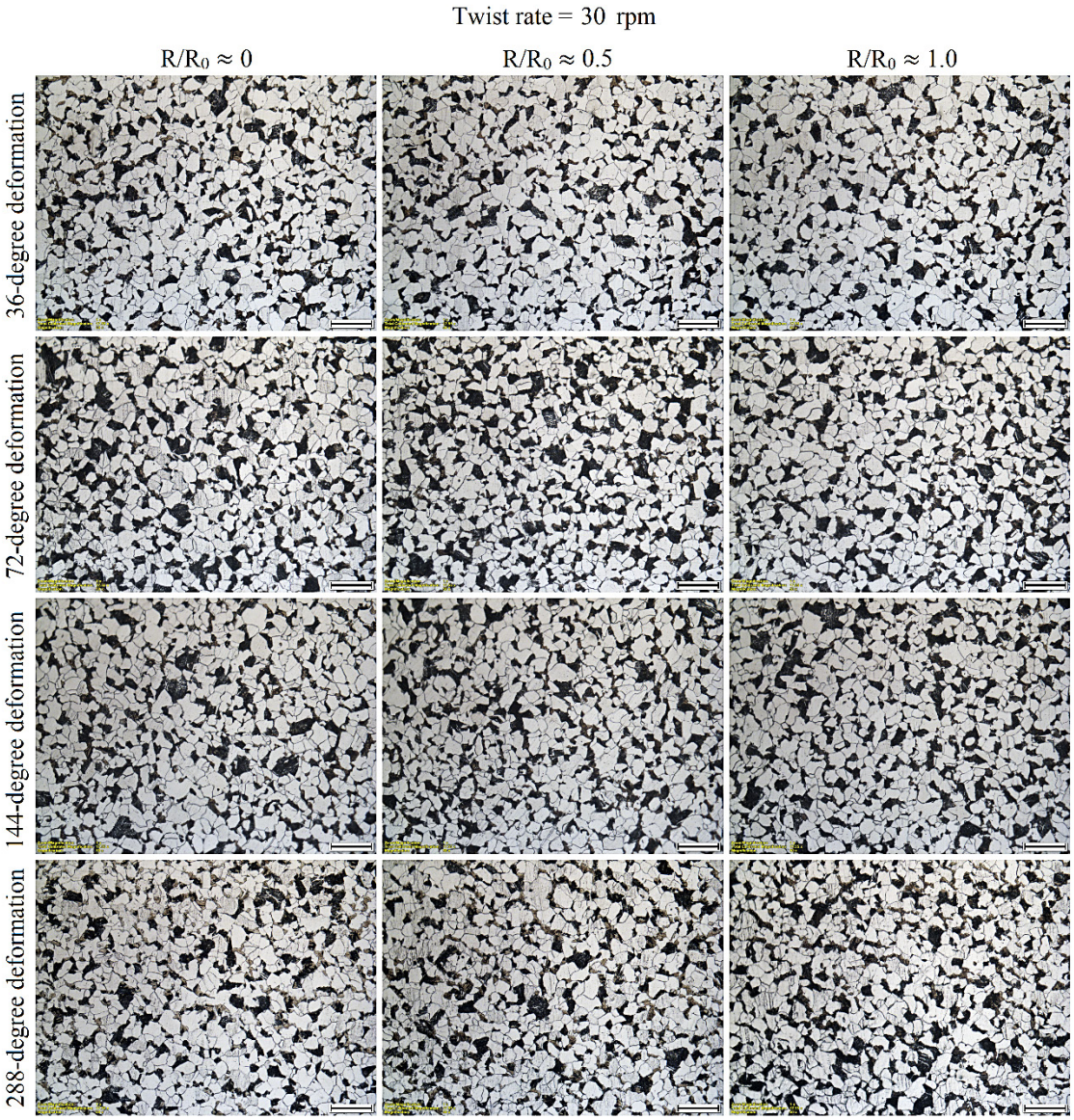

Figure 9 Light optical micrographs at various R/R_0 positions of specimens with pre-torsional deformation to various angles at a twist rate of 30 rpm (scale bar = 50 μm).

Table 4 Average grain size of specimens with different pre-torsional conditions at various R/R_0 positions away from the specimen's axial centerline along its radial direction.

Pre-torsional condition	Average grain size (μm)		
	$R/R_0 \approx 0.0$	**$R/R_0 \approx 0.5$**	**$R/R_0 \approx 1.0$**
No pre-torsional deformation	20.9 ± 5.8	20.5 ± 5.1	20.2 ± 5.6
36 degrees at 0.1 rpm	20.8 ± 5.3	20.1 ± 4.5	19.5 ± 5.9
72 degrees at 0.1 rpm	19.4 ± 5.5	19.9 ± 6.4	18.7 ± 6.8
144 degrees at 0.1 rpm	19.8 ± 5.9	20.4 ± 5.3	19.5 ± 5.4
288 degrees at 0.1 rpm	20.5 ± 5.7	20.8 ± 6.9	20.1 ± 6.1
36 degrees at 30 rpm	21.2 ± 5.2	20.6 ± 6.2	20.9 ± 5.8
72 degrees at 30 rpm	19.1 ± 4.5	19.5 ± 6.4	19.7 ± 6.5
144 degrees at 30 rpm	20.9 ± 5.9	21.2 ± 5.8	20.2 ± 5.1
288 degrees at 30 rpm	21.7 ± 6.3	21.3 ± 4.9	19.9 ± 5.9

Based on the tensile and hardness tests, pre-torsional deformation enhanced yield and tensile strengths and local hardness, but reduced ductility, strain hardening rate, work hardening capacity, known as strengthening effect. The hardening effects via severe plastic deformation such as pre-torsional deformation are originated from either or both of the following 2 strengthening mechanisms: (i) strain hardening (ii) grain-size strengthening. Though both mentioned mechanisms enhance strength and hardness through hindering dislocation motion, strain hardening is a result of the dislocation accumulation and entanglement within the grains' interior during plastic deformation while grain-size strengthening utilizes an increase in grain boundaries after grain-size reduction through grain refinement [11,21]. Since the average grain sizes were uniform throughout the specimens in the radial direction and the differences in the average grain size among all pre-torsional conditions were statistically insignificant, it is concluded that the principal strengthening mechanism involving pre-torsional deformation of hot-rolled SCM415 steel is strain hardening.

Moreover, a gradient in local hardness after pre-torsional deformation along the radial direction, where the hardness was highest near the surface region while lowest near the central region, was observed. This is because the strain hardening is a function of the amount of plastic strain caused by the cold forming process and the shear strain (γ) caused by torsion in a cylinder is proportional to the distance away from the center of the cylinder, which is expressed in the Eq. (4) as follows [22]:

$$\gamma = \frac{R}{L}.\frac{\pi\theta}{180} \tag{4}$$

where R is the distance from the specimen's center, L is the gauge length of the specimen, and θ is the torsional angle in degree.

Lastly, the higher shear strain rate during pre-torsional deformation amplifies the strain hardening effect. This is due to higher shear strain rate via faster twist rate restricts the dynamic recovery process involving dislocation climb and annihilation [23,24,25]. Since the dynamic recovery reduces the dislocation density accumulated during plastic deformation, a faster twist rate leads to higher dislocation density after pre-torsional deformation, hence, further enhancing the strength and hardness of hot-rolled SCM415 steel.

Conclusions

Hot-rolled SCM415 round tensile specimens based on ASTM E8M standard were pre-torsionally deformed by a free-end torsion tester at room temperature to 36, 72, 144, and 288 degrees at 2 different twist rates of 0.1 and 30 rpm. After tensile tests of specimens before and after pre-torsional deformation, engineering stress-strain curves showed that yield strength and ultimate tensile strength increased while ductility decreases with higher torsional angles and higher twist rates. The strain hardening rates were lower with increasing torsional angle and twist rate. Within uniform plastic deformation region, the relationship of true stress and true strain was well described by a power law for all pre-torsional conditions. The power-law parameters, namely strength coefficient (K) and strain hardening exponent (n) decreased with increasing amount of shear plastic strain and shear strain rate during the pre-torsional deformation. In pre-torsioned specimens, local Vicker hardness showed a positive gradient from the central region to the surface. The local hardness at the same distance from the center increased with increasing torsional angle and twist rate. Based on the light optical micrographs, the average grain sizes of pre-torsioned specimens were found to be unaffected by the amount of torsional angle or the rate of twist. Therefore, strengthening of hot-rolled SCM415 steel via pre-torsional deformation is predominated by strain hardening suspectedly through dislocation accumulation and entanglement within the grains' interior. Furthermore, high shear strain rate was found to limit the dynamic recovery process, resulting in further enhancing the strain hardening effects.

Acknowledgements

This research was funded by College of Industrial Technology, King Mongkut's University of Technology North Bangkok, Thailand (Grant No.: Res-CIT0263/2020).

References

[1] LV Long, DV Hien, NT Thanh, NC Tho and VT Do. Impact of cold-rolling and heat treatment on mechanical properties of dual-phase treated low carbon steel. *Adv. Mater. Sci. Eng.* 2020; **2020**, 1674837.

[2] TY Wang, RB Song, HJ Cai, J Wen and Y Su. Influence of cold rolling reduction on microstructure and mechanical properties in 204C2 austenitic stainless steel. *Mater. Sci. Forum* 2019; **944**, 193-8.

[3] AC Umamaheshwer Rao, V Vasu, M Govindaraju and KV Sai Srinadh. Influence of cold rolling and annealing on the tensile properties of aluminum 7075 alloy. *Procedia Mater. Sci.* 2014; **5**, 86-95.

[4] NA Raji and OO Oluwole. Influence of degree of cold-drawing on the mechanical properties of low carbon steel. *Mat. Sci. App.* 2011; **2**, 1556-63.

[5] MC Nebbar, M Zidani, T Djimaoui, T Abid, H Farh, T Ziar, AL Helbert, F Brisset and T Baudin. Microstructural evolutions and mechanical properties of drawn medium carbon steel wire. *Int. J. Eng. Res. Afr.* 2019; **41**, 1-7.

[6] SH Huang, Y Wu, XS Xia, ZD Zhao, Q Chen and DY Shu. Assessment of cold extrusion effect on stress-strain curves of pure copper arc parts based on the cosine velocity model. *Strength Mater.* 2019; **51**, 569-77.

[7] SJ Liang, ZY Liu and ED Wang. Microstructure and mechanical properties of Mg-Al-Zn alloy deformed by cold extrusion. *Mater. Lett.* 2008; **62**, 3051-4.

[8] L Wang, W Lu, J Qin, F Zhang and D Zhang. Microstructure and mechanical properties of cold-rolled TiNbTaZr biomedical β titanium alloy. *Mater. Sci. Eng. A* 2008; **490**, 421-6.

[9] X Zhang, A Godfrey, X Huang, N Hansen and Q. Liu. Microstructure and strengthening mechanisms in cold-drawn pearlitic steel wire. *Acta Mater.* 2011; **59**, 3422-30.

[10] WDJR Callister. and DG Rethwisch. *Materials science and engineering: An introduction*. 10th eds. Wiley, New Jersey, 2018.

[11] C Wang, F Li, J Li, J Dong and F Xue. Microstructure evolution, hardening and thermal behavior of commercially pure copper subjected to torsion deformation. *Mater. Sci. Eng. A* 2014; **598**, 7-14.

[12] C Wang, F Li, L Wang, H Qiao. Review on modified and novel techniques of severe plastic deformation. *Sci. China Technol. Sci.* 2012; **55**, 2377-90.

[13] RZ Valiev, RK Islamgaliev and IV Alexandrov. Bulk nanostructured materials from severe plastic deformation. *Prog. Mater. Sci.* 2000; **45**, 103-189.

[14] T Ungár, LS Tóth, J Illy and I Kovács. Dislocation structure and work hardening in polycrystalline ofhc copper rods deformed by torsion and tension. *Acta Metall.* 1986; **34**, 1257-67.

[15] J Gu, L Zhang, S Ni and M Song. Effects of grain size on the microstructures and mechanical properties of 304 austenitic steel processed by torsional deformation. *Micron* 2018; **105**, 93-7.

[16] H Chen, F Li, J Li, Z Zhao, S Zhou and Q Wan. Experimental study on pure titanium during the positive-torsion and positive-negative-torsion. *Mater. Sci. Eng. A* 2016; **674**, 552-68.

[17] JH Hollomon. Tensile deformation. *Trans. Am. Inst. Mech. Eng.* 1945; **162**, 268-77.

[18] M Bruneau, CM Uang and R Sabelli. *Ductile design of steel structures*. 2nd eds. McGraw-Hill, New York, 2011.

[19] WF Hosford and RM Caddell. *Metal Forming: Mechanics and metallurgy*. 4th eds. Cambridge University Press, New Jersey, 2011.

[20] JA Schey. *Introduction to manufacturing processes*. 3rd eds. McGraw-Hill, New York, 2000.

[21] J Gu, S Ni and M Song. Mechanical properties and microstructural evolution of CuZn alloys via pre-torsional deformation. *Mat. Res.* 2019; **22**, e20180424.

[22] R Pippan, F Wetscher, M Hafok, A Vorhauer and I Sabirov. The limits of refinement by severe plastic deformation. *Adv. Eng. Mater.* 2006; **8**, 1046-56.

[23] W Blum and XH Zeng. A simple dislocation model of deformation resistance of ultrafine-grained materials explaining Hall-Petch strengthening and enhanced strain rate sensitivity. *Acta Mater.* 2009; **57**, 1966-74.

[24] Z Zhang, Q Dong, B Song, H He, L Chai, N Guo, B Wang and Z Yao. Effect of shear strain rate on microstructure and properties of austenitic steel processed by cyclic forward/reverse torsion. *Materials* 2019; **12**, 506.

[25] RC Souza, ES Silva, AMJR Jorge, JM Cabrera and O Balancin. Dynamic recovery and dynamic recrystallization competition on a Nb- and N-bearing austenitic stainless steel biomaterial: Influence of strain rate and temperature. *Mater. Sci. Eng. A* 2013; **582**, 96-107.